ACS APPLIED MATERIALS & INTERFACES

Research Article

www.acsami.org

Low Cost Facile Synthesis of Large-Area Cobalt Hydroxide Nanorods with Remarkable Pseudocapacitance

Ming-Jay Deng,*[,†,§] Cheng-Zhao Song,[†,‡,§] Chien-Chia Wang,[†,‡] Yuan-Chieh Tseng,[‡] Jin-Ming Chen,*[,†] and Kueih-Tzu Lu*[,†]

[†]National Synchrotron Radiation Research Center (NSRRC), Hsinchu, Taiwan

[‡]Department of Materials Science and Engineering, National Chiao Tung University, Hsinchu, Taiwan

Supporting Information

ABSTRACT: Large-area $Co(OH)_2$-based supercapacitor electrodes composed of nanotube arrays grown on a 3D nickel-foam (CONTA) electrode and sucker-like nanoporous films grown on a 3D nickel-foam (COSNP) electrode were prepared with a facile electrochemical method for applications in energy storage. These nanoporous $Co(OH)_2$ electrodes were fabricated with the codeposition of Cu/Ni film on the nickel foam, then etching of Cu from the Cu/Ni layer to form Ni nanotube arrays and sucker-like Ni nanoporous layers, and further cathodic deposition of $Co(OH)_2$ on the prepared nanoporous Ni substrates. The CONTA and COSNP electrodes exhibited specific capacitances of 2500 and 2900 F/g in a voltage range of 0.65 V (capacitance of the substrates deducted from the total) at 1 A/g in a three electrode cell, respectively. The COSNP electrode demonstrated an excellent supercapacitive performance with specific capacitances 1100 F/g at 1 A/g and 850 F/g at 20 A/g in a voltage range of 1.2 V in a two electrode cell. The remarkable performance of COSNP electrodes correlated with a large conversion of the Co oxidation state during the charge/discharge cycling were examined by *in situ* X-ray absorption near edge structure (XANES).

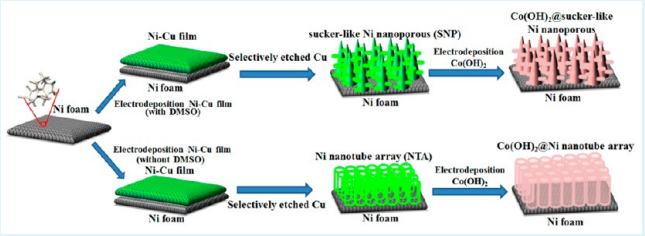

KEYWORDS: *cobalt hydroxide, symmetric supercapacitor, nanotube, nanoporous*

1. INTRODUCTION

With ever-increasing global warming and the approaching depletion of fossil fuels, a target of much research is to develop sustainable and renewable clean production of alternative energy from the sun, wind, and so on.[1−5] Among all advanced battery systems, lithium-ion batteries have captured the movable electronic market, but to serve the upcoming markets for energy storage on a large scale, much improved capacity of energy storage is immediately needed.[3−6] In recent years, electrochemical capacitors (ECs) have obtained great attention as an important device to store energy owing to their large power densities, good life-cycle, and fast-recharge capability.[1−6] They have hence became progressively attractive for use in global customer electronics, devices for hybrid electric vehicles, and medical systems. Pseudocapacitors, in which the capacitance is recognized dominantly to the reversible and continuous oxidation/reduction reactions of electrodes as an intermediate system between Li-ion batteries and dielectric capacitors,[1−4] have attracted considerable attention because not only are the corresponding energy densities better than those of typical carbonaceous materials with electric double layer capacitors but also their power densities are greater than those of Li-ion batteries. Carbon materials—carbon nanotubes, graphene, activated carbon and mesoporous carbon nanowires[7−9]—provide electric double-layer capacitors with specific capacitance (C_{sp}) generally smaller than 250 F/g, and also small energy densities because the corresponding energy storage is constructed on the offered active surface area.[2] Transition metal oxides are attractively recognized as promising materials for pseudocapacitors because they enable offering several oxidation states for useable charge storage with oxidation/reduction reactions to reach great performances.[1,2,5] Hydrous RuO_2 is one of the famous materials with great capacitances;[10,11] however, its toxic nature and high cost limit its commercial use. Among other transition metal oxides, $Co(OH)_2$ can be a hopeful material as a material alternative to RuO_2 because of its environmentally benign nature, low cost, great theoretical capacitance (larger than 3000 F/g), structural property, tunable surface, controllability of the shape or the size, excellent electrochemical performance in alkaline solutions through the capability to interact with the ions in electrolytes not only all over the surface but also in the bulk, and then beneficial pseudocapacitive performances.[12] Some C_{sp} of $Co(OH)_2$ even exceed those of RuO_2,[13,14] but most observed specific capacitances for $Co(OH)_2$ are normally less than 1000 F/g.[15−21] The poor electrical conductivity of $Co(OH)_2$ increases both the charge transfer resistance and the sheet resistance of these electrodes, which, in work reported to date, has led to a

Received: February 9, 2015
Accepted: April 15, 2015
Published: April 15, 2015

DOI: 10.1021/acsami.5b01163
ACS Appl. Mater. Interfaces 2015, 7, 9147−9156

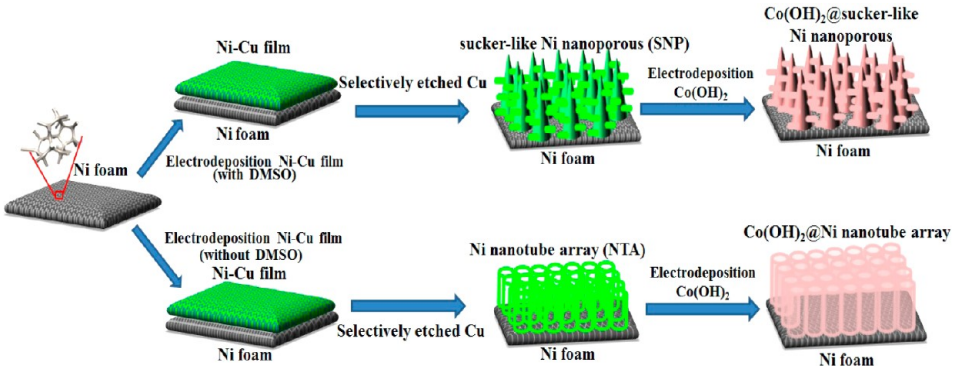

Figure 1. Scheme of electrochemical preparation of highly porous nanoarchitectured $Co(OH)_2$ electrodes.

capacitance much less than the theoretical value and a poor rate capability.[14,16,22] Various methods, such as modification with nanostructured carbon and synthesis of nanostructures with unique morphology, have thus been applied in attempts to improve the $Co(OH)_2$ supercapacitor performance.[16−22] Despite the extensive research, there is a noteworthy barrier to the performance of these pseudocapacitors; namely, the restricted capability of the continuous cyclability, charge/discharge performance, and a large scale.

The capability of EC is governed principally by its electrochemical kinetics and activity of the electrode. As a result, to develop the performance of ECs at large rates, it is of great importance to raise the rates of electron transport in electrode and electrolyte ions and at the electrolyte/electrode interfaces and to contain sufficiently electro-active materials disclosed on the surface for the faradaic oxidation/reduction reaction.[16] An ideal scheme is binder-free (self-supported) nanoarchitectured electrodes, which are normally constructed as one dimension or two dimension toy bricks and directly made on the current collector. This type of electrode is typically expected to bestow various benefits, for example low diffusion resistance to ionic species, satisfactory electrical conductivity, huge electro-active surface area, and easy electrolyte penetration.[23−28] More exactly, pathways of both electrons and electrolyte ions in these nanoarchitectured electrode materials are simultaneously built to enable effective energy storage at large rates, to realize a maximum application of electro-active electrodes at high current density.

We here describe a facile electrochemical synthesis of 3D $Co(OH)_2$ based nanoarchitectured electrode materials with great capacitance, satisfactory rate capability, and a large area. To confirm the rapid diffusion of ions and hence the enhanced efficiency of electrolyte penetration, we employed a Ni foam substrate with uniform and large pores, large electrical conductivity, and huge supporting area as the current collector; the arrays of Ni nanotubes (NTA) and sucker-like Ni nanopores (SNP) were grown on 3D nickel foam. $Co(OH)_2$ was further grown vertically on these substrates to form the CONTA and COSNP electrodes, respectively, leaving many macro-meso-micropores for ion access and transport. The preparation of the 3D $Co(OH)_2$-based nanoarchitectured electrodes is a fully electrochemical procedure (see Figure 1). It has many benefits of simplicity, reliability, great accuracy, and low-cost.[23−29] Both CONTA and COSNP electrodes thus exhibit specific capacitances 2500 and 2900 F/g at 1 A/g, respectively, based on the total mass of $Co(OH)_2$ (very close to the theoretical value of 3450 F/g)[14] in solution (KOH, 1 M) in the potential range from −0.2 to +0.45 V (vs SCE). As the current density is increased to 20 A/g, the C_{sp} of 1800 and 2360 F/g of CONTA and COSNP electrodes, respectively, are maintained, indicating the superior power performance. A satisfactory cycling performance and high-rate capability were verified in these electrodes. We compared the pseudocapacitive behavior of the flake-like $Co(OH)_2$/Ni foam electrode and explained the change of oxidation state of Co ions of these different electrodes in KOH solution with *in situ* XANES. The supercapacitor displays efficient charge compensation in the $Co(OH)_2/CoO_2$ redox reaction during charge/discharge cycles with a great change of ∼1.79 of the Co oxidation state.

2. EXPERIMENTAL SECTION

2.1. Materials Synthesis. All chemicals were of reagent quality and used without an extra purification. Nickel foam (area ∼50 cm^2) was etched in HCl (1M), soaking in $NiCl_2$ (0.01 M), washed with water in an ultrasonic bath, and used as the working electrode after drying so that effective adhesion was obtained. Cu/Ni films were further electrodeposited on the nickel foam substrate from the solution containing $NiCl_2$ (0.5 M), $NiSO_4$ (0.5 M), $CuSO_4$ (0.01 M), H_3BO_3 (1 M, pH = 3.8), and dimethyl sulfoxide (DMSO, 5%), or without DMSO. All electrodeposition was performed at 27 °C in three electrode system with the platinum counter electrode and the saturated calomel reference electrode (SCE). The Cu/Ni layer was electrodeposited at −0.78 V; the total deposited charge was measured at 150 C. Then Cu was selectively dissolved from the electrodeposited Cu/Ni layer at 0.8 V until 15 $\mu A/cm^2$ to grow the Ni nanoporous film. The loading amount of Ni nanoporous film (exclude the Ni foam) was on average 15 mg or 0.3 mg cm^{-2} (XP105DR Mettler Toledo).

2.2. Materials Characterization. All nanoporous samples were analyzed with the energy dispersive spectroscope (EDS), scanning electron microscope (SEM, JEOL 6500F), and transmission electron microscope (TEM, JEOL 2000F). The crystal structure was measured by X-ray diffraction (XRD) techniques at BL01C2 of NSRRC, and the XRD peaks were changed to Cu Kα X-ray radiation. The change of the Co oxidation state in these electrodes was considered at several potentials in solution with Co K-edge XANES spectra recorded in the fluorescence yield mode. An electrochemical cell with the Kapton window transparent to fluorescence was adopted. Before studying the absorption spectrum at an applied potential, we kept the working electrode at the established potential for 20 min to permit the COSNP to get the steady state. Co K-edge XANES experiments were conducted at BL17C1 and 01C1. All of the X-ray absorption energies were calibrated with a Co K-edge absorption inflection point at 7709 eV of the Co foil, which were estimated before every test. X-ray photoemission spectroscopy (XPS) was also applied to probe the Co oxidation state at BL20A.

2.3. Electrochemical Measurements. $Co(OH)_2$ was cathodically deposited on the surface of the developed nanoporous Ni substrate materials in the solution containing $Co(NO_3)_2$ (0.1 M), $Co(CH_3COO)_2$ (0.1 M), NH_4NO_3 (0.05 M), and $NaNO_3$ (0.05M). A

DOI: 10.1021/acsami.5b01163
ACS Appl. Mater. Interfaces 2015, 7, 9147−9156

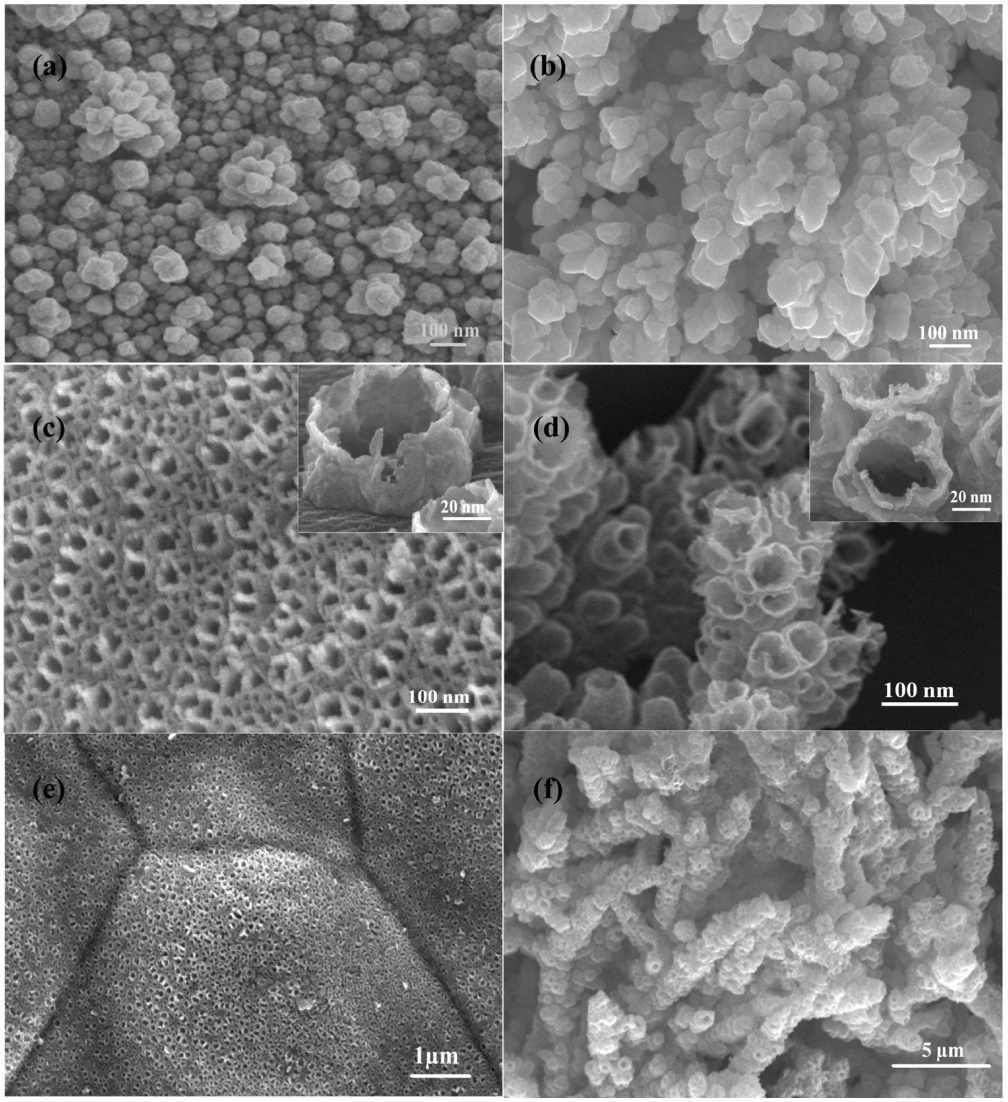

Figure 2. High magnification SEM images of the Ni−Cu alloy films as deposited on nickel foam obtained on constant potential electrodeposition at −0.78 V (a) in solution (without DMSO) and (b) in solution (containing DMSO, 5%). (c,d) High magnification SEM images of the Ni nanostructure films after Cu was selectively etched from a and b, respectively. (e,f) Low magnification SEM images from c and d, respectively.

cathodic potential of −0.7 V was used to produce the total conducted charge of 60 C. The loading amount of $Co(OH)_2$, on average 25 mg (or 0.5 mg cm^{-2}), was weighed with the microbalance (XP105DR Mettler Toledo) at an accuracy of 0.01 mg. The same amount of $Co(OH)_2$ was electrodeposited on nickel foam to make the counterpart electrode. Electrochemical performances of these electrodes were measured in KOH solution (1 M, 27 °C) using cyclic voltammetry (CV); it was carried out in the potential range −0.2 to +0.45 V (vs SCE) at scan rates of 10 mV/s. An electrochemical impedance spectroscopy (EIS) experiment was studied using the frequency range from 0.1 Hz to 100 kHz with an amplitude of 10 mV. All electrochemical measurements were made with a potentiostat (AUTOLAB). Electrochemical performances of these assembled symmetrical supercapacitor devices were also investigated via CV and charge/discharge measurements in two electrode system, wherein KOH solution (1 M) served as electrolyte and a cellulose paper membrane served as separator. The symmetric device was tested with the voltage range 0 to 1.2 V using CV and charge/discharge methods at various current densities.

3. RESULTS AND DISCUSSION

3.1. Characterization. Figure 1 illustrates our research strategy for the $Co(OH)_2$-based electrodes composed of nanotube arrays grown on a 3D nickel foam (CONTA) electrode and sucker-like nanoporous films grown on a 3D nickel foam (COSNP) electrode with a facile electrochemical method. The electrochemically synthesized nanotube arrays (NTA) or sucker-like nanoporous films (SNP) aid as the mainstay for the succeeding electrodeposition of $Co(OH)_2$ nanorods. The resulting NTA or SNP can be electrodeposited on nickel foam substrates. Figure S1 (in the Supporting Information) displays two CV curves of nickel foam electrodes studied in a solution ($NiSO_4$ 0.5 M, $NiCl_2$ 0.5 M, $CuSO_4$ 0.01 M, H_3BO_3 1 M) with 5% dimethyl sulfoxide (DMSO) or without DMSO, respectively. In light of Figure S1, the electrodeposition of Cu/Ni films and hence etching of Cu from Cu/Ni films were finished in the original solution with merely exchanging the potential at −0.78 or 0.8 V. The SEM morphologies of NTA and SNP on the nickel foam substrate are presented in Figure 2. Figure 2a and b show images of Cu/Ni layers electrodeposited at −0.78 V with a charge of 3 C/cm^2. Figure 2a displays the granular image of the electrodeposited layer from the plating solution without DMSO, of which the Cu/Ni atomic ratio was roughly 55:45 (verified by EDS). In

DOI: 10.1021/acsami.5b01163
ACS Appl. Mater. Interfaces 2015, 7, 9147−9156

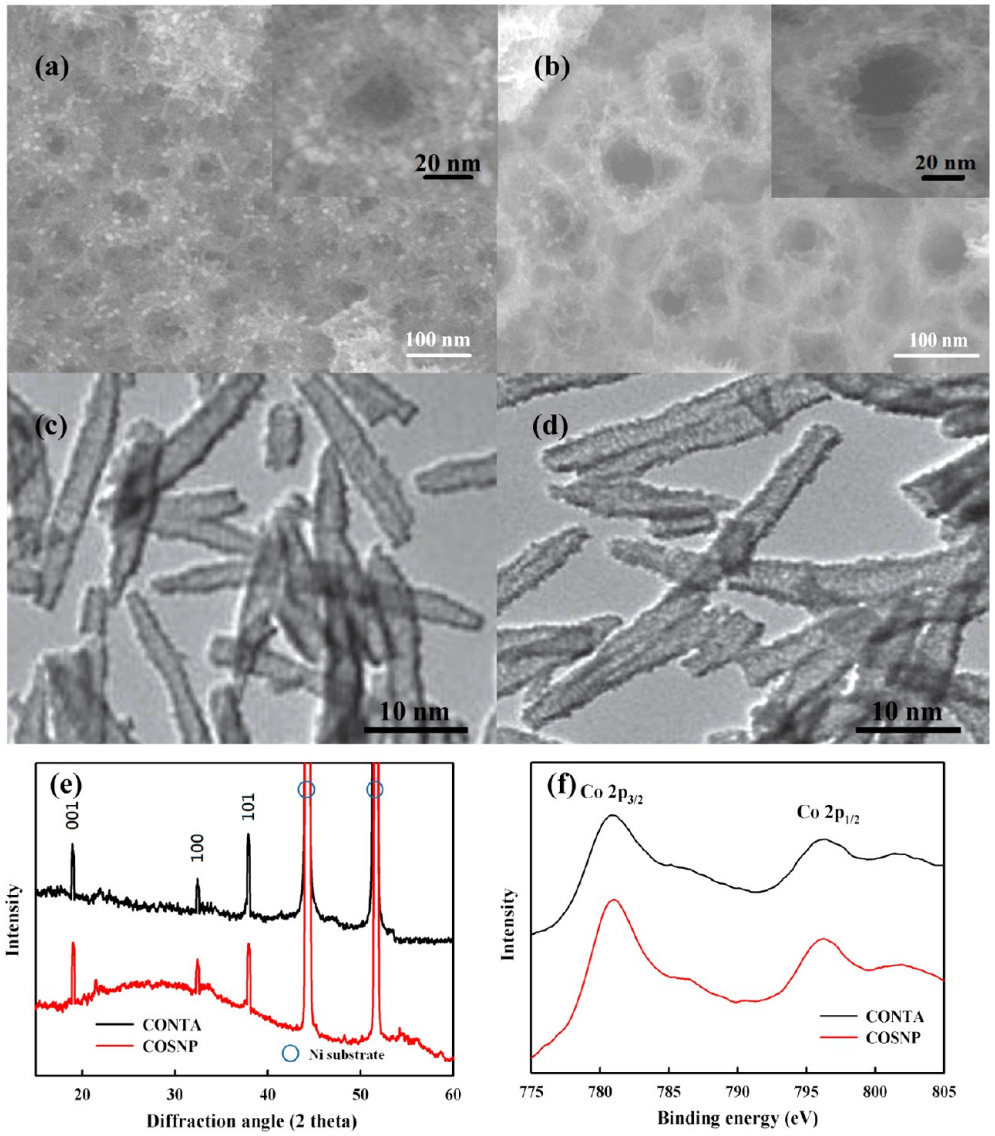

Figure 3. High magnification SEM images of (a) the $Co(OH)_2$ nanorods grown on NTA and (b) the $Co(OH)_2$ nanorods grown on SNP. (c,d) TEM images of the $Co(OH)_2$ nanorods from a and b, respectively. (e) XRD patterns for $Co(OH)_2$ nanorod films; (f) Co 2p XPS spectra of the $Co(OH)_2$ nanorod films.

Figure 2b, through the film deposited from the plating solution containing DMSO (5%), fresh granules appeared to form on earlier ones, developing into a protuberant architecture (Cu/Ni atom % = 55/45). The granules inclined to collect and overlay into bunches when total charge was enhanced. Figure 2c and d display the nanostructures established from the Cu/Ni layers in Figure 2a and b when being etched at 0.8 V. As presented in Figure 2c, an NTA of diameter of about 50 nm and a pore density of approximately 10^{13} cm^{-2} were observed. As shown in Figure 2d, the morphologies gradually became SNP structures, because the bunching of the Cu/Ni granules caused formation of interconnected pores above etching. The layers with pore sizes range from 30 to 80 nm and have a thickness of about 5 μm. The microscopic analyses showed that the NTA and SNP with great density grew uniformly on the skeletons of the nickel-foam substrate, as presented in Figure 2e and f, developing the hierarchical structure. Nickel foam adhered much more effectively to the NTA and SNP than to a flat substrate. As a thicker film formed, a 3D hierarchically porous structure appeared more attainable. In Figure S2a, XRD patterns of Cu/Ni films without and with DMSO before and after etching at 0.8 V reveal that Cu portion was eliminated. Figure S2b displays Cu $2p_{3/2}$ XPS spectra taken from films electrodeposited at −0.78 V without and with DMSO (5%). The XPS signal of binding energy (932.7 eV) corresponds to zero-valent Cu.[30] After etching, the samples were analyzed also with XPS, as presented in Figure 3b. As presented, the Cu $2p_{3/2}$ peak intensity significantly reduced after etching. These effects verify that, because of the conformation of oxide layers in the plating solution, Ni transformed, passivated, and maintained on the nickel foam, whereas Cu was eliminated under anodic potential. These given in Figures 2 and S2 show that the central portion was Cu and was preferentially etched when anodic potential was employed, creating hollow Ni nanostructures, such as NTA or SNP. Chemical separation in deposited Cu/Ni granules was noticed in previous literature.[31,32] As a result, we have prepared a quick electrochemical method to create Ni nanostructures. The NTA and SNP with a porosity of 3D were applied to load $Co(OH)_2$ nanorods.

DOI: 10.1021/acsami.5b01163
ACS Appl. Mater. Interfaces 2015, 7, 9147−9156

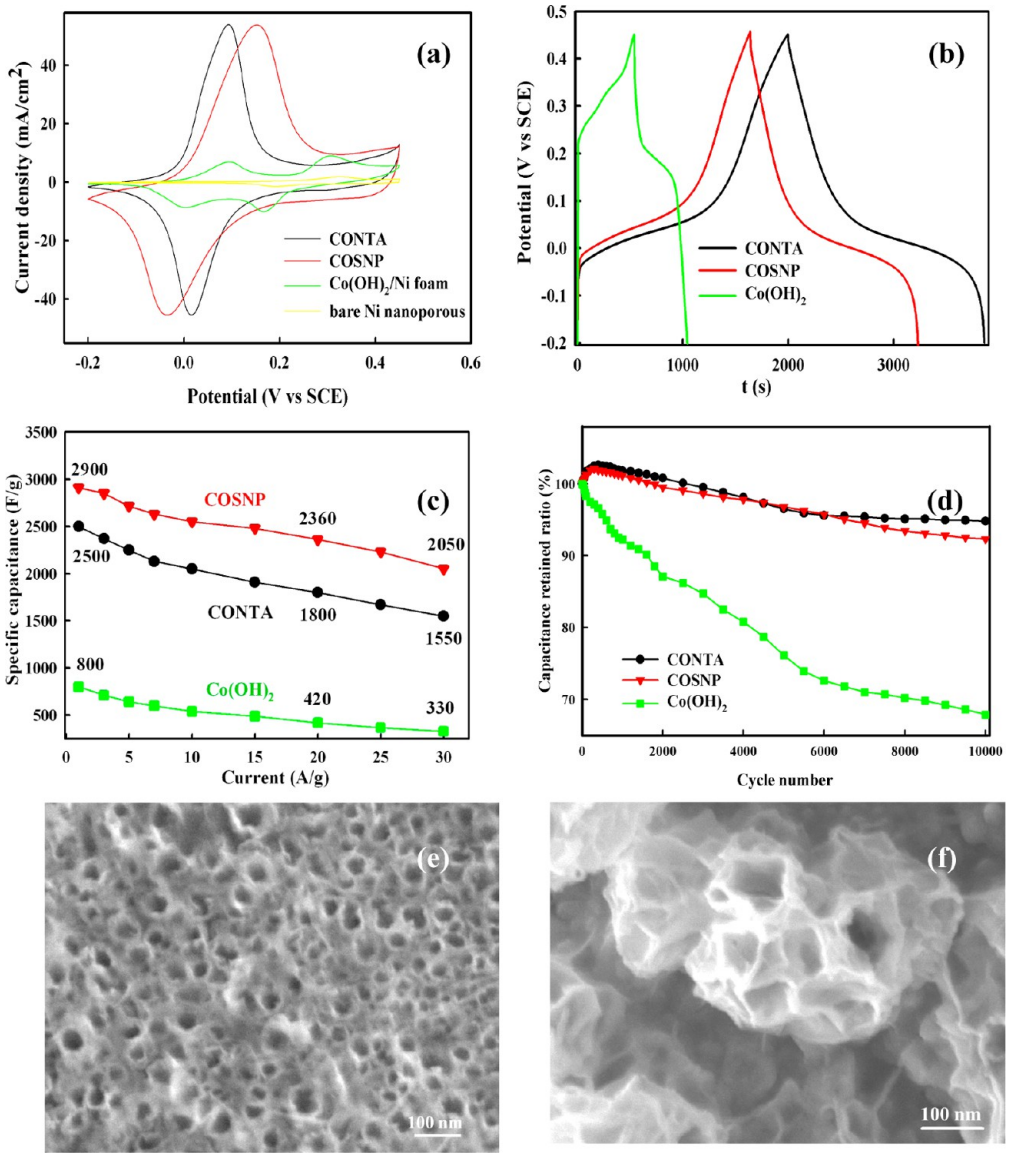

Figure 4. Electrochemical characterization of CONTA, COSNP, and $Co(OH)_2$ electrodes recorded in the KOH solution. (a) CV curves of these electrodes at a scan rate of 10 mV s^{-1}. (b) Galvanostatic charge−discharge curves of these electrodes at the same current density of 1 A g^{-1}. (c) Specific capacitance as a function of current density. (d) Long-term cycling performance of these electrodes. SEM images of (e) CONTA and (f) COSNP electrodes after 10 000 cycles.

To achieve an entirely electrochemical construction of a nanoporous supercapacitor electrode, we tried deposition of $Co(OH)_2$ nanorods on the prepared NTA and SNP. Figure 3a and b show the image of cathodically electrodeposited $Co(OH)_2$ nanorods on developed NTA and SNP templates, respectively. As these figures show, $Co(OH)_2$ nanorods of a width of only a few nanometers were uniformly dispersed on nanosize Ni tubes and Ni suckers, respectively, even inside pores, growing micro-, meso-, and macroporous architecture. The thickness of the $Co(OH)_2$ layer is ∼40 nm on the surface of nanosize Ni tubes and Ni suckers, respectively. The evidence appears to support that the $Co(OH)_2$ electrodes as prepared have a 3D hierarchically porous structure throughout the entire layer with great surface area. The TEM images shown in Figure 3c and d demonstrate that the products have rod-like nanostructures. The structural information and purity of the samples were further characterized by XRD measurements, as presented in Figure 3e. Besides two strong peaks related with the nickel substrate shown in Figure 3e, the XRD pattern of $Co(OH)_2$ nanorods displays a brucite-like phase, corresponding to the peak positions (JCPDS No. 30-0443) wherein the diffraction peaks at 19.0°, 32.4°, and 37.9° conform to the (001), (100), and (101) peaks. Further evidence for the chemical state of the $Co(OH)_2$ nanorods as deposited was acquired from XPS, as displayed in Figure 3f. The Co 2p XPS shows two main features at 781 and 796.2 eV, conforming to Co $2p_{3/2}$ and Co $2p_{1/2}$, respectively. These features endorse the existence of the Co(II) state in CONTA and COSNP electrodes as prepared, which matches the previous reference.[33] On the basis of these results, the 3D $Co(OH)_2$ nanorods as deposited are fabricated successfully in our work. Figure S3 displays the SEM image of unmodified $Co(OH)_2$ electrodes with nickel foam substrates. On the nickel foam substrate, $Co(OH)_2$ nanostructures were watched to compose uniform and highly porous nanoflake-like film, which fully covered the skeleton of nickel foam. The BET surface area of these

DOI: 10.1021/acsami.5b01163
ACS Appl. Mater. Interfaces 2015, 7, 9147−9156

electrodes was determined to be 98 $m^2 g^{-1}$ (normalized by the mass of $Co(OH)_2$) for unmodified $Co(OH)_2$, 163 $m^2 g^{-1}$ for the CONTA, and 198 $m^2 g^{-1}$ for the COSNP electrode (see Figure S4, Supporting Information). BET tests were finished by studying the entire architecture, and thus, minus the blank nickel foam. Such CONTA and COSNP with 3D nanostructures and large specific surface areas have the greatest probability to deliver a great performance in biosensors, electrochemical sensors, and ECs.

3.2. Electrochemical Characterization. To explore the mechanism of energy storage and electrochemical capability of these $Co(OH)_2$ electrodes as deposited, we employed CV and charge/discharge measurements in KOH aqueous solution with the three electrode cell. The C_{sp} based on CV and the charge/discharge cycle can be measured as follows:

$$C_{sp} = Q_m/\Delta V \quad (1)$$

$$C_{sp} = I\Delta t/\Delta V w \quad (2)$$

where Q_m denotes the specific voltammetric charge combined from CV (the mass of $Co(OH)_2$), ΔV is the potential range (0.65 V × 2), I is the applied constant current density (1 A/g), Δt is the duration of the charge/discharge cycling, and w is the mass of $Co(OH)_2$. CV curves for these $Co(OH)_2$ electrodes as deposited at a scan rate of 10 mV/s with a scan range from −0.2 to +0.45 V are shown in Figure 4a. The CV consists of a pair of strong oxidation/reduction peaks over the full scan range. The result shows that capacitance features are mostly controlled by faradaic oxidation/reduction reactions and not by simple double layer capacitance. A large oxidation/reduction current and noticeable oxidation/reduction peaks indicate outstanding pseudocapacitive performance for CONTA and COSNP electrodes. Figure 4a also displays a CV of the unmodified $Co(OH)_2$ electrode. Through the scan result, two smaller redox couples superimposed on the wide oxidation/reduction background were identified, also meaning that reversible pseudocapacitive redox processes of $Co(OH)_2$ were included. On the basis of the literature, faradaic oxidation/reduction reactions happening on the surface of $Co(OH)_2$ electrodes can be expressed as follows:[14−18]

$$Co(OH)_2 + OH^- \leftrightarrow CoOOH + H_2O + e^- \quad (3)$$

and reactions beyond the oxidation/reduction peaks at slightly larger potentials can be presented as follows:

$$CoOOH + OH^- \leftrightarrow CoO_2 + H_2O + e^- \quad (4)$$

As shown in Figure 4a, the currents of the CONTA and COSNP electrodes are much greater than those unmodified $Co(OH)_2$ electrodes, representing that CONTA and COSNP electrodes have great electrochemical reaction activity, which also conforms to the performance. The bare Ni nanoporous substrate was not immensely exposed to an electrolyte and contributed to an evident oxidation/reduction signal in Figure 4a. The C_{sp}'s of these electrodes were calculated from CVs corresponding to eq 1. The calculated C_{sp}'s of CONTA and COSNP electrodes are ∼2500 and ∼2900 F/g (based on the mass of $Co(OH)_2$), respectively. In contrast, unmodified $Co(OH)_2$ electrode displays a C_{sp} of merely ∼800 F/g, which is near that normally reported from the literature.[15,16,18−22] The evidence appears to support that a superior pseudocapacitance results from the 3D hierarchical nanoarchitecture. In particular, the introduction of a 3D SNP structure into the $Co(OH)_2$ electrode caused an increased maximum current, which is answerable for a charge performance greater than that of the unmodified $Co(OH)_2$ electrode. Figure 4b displays the comparison of charge/discharge voltage−time profiles for the CONTA, COSNP, and $Co(OH)_2$ electrodes at 1 A/g. The results consistent with CV and the plateaus in charge/discharge curves also represent the presence of faradaic reactions. The charge/discharge curves of COSNP and CONTA are extremely symmetrical without a noticeable i_R drop at lower current density, meaning a quick $I-V$ reply and outstanding electrochemical reversibility. According to eq 2, the C_{sp} of the CONTA and COSNP electrodes were calculated to be 2500 and 2900 F/g, respectively, which are 3-fold higher than that of the $Co(OH)_2$ electrode (800 F/g) and which were close to the values from CV, again confirming the surprising capacity for energy storage. Even though the value is less than the theoretical value for $Co(OH)_2$ (about 3460 F/g),[14] it is greater than other $Co(OH)_2$ electrodes.[15−22] Figure S5 presents charge/discharge curves of the COSNP electrode at various current densities as indicated. A sluggish decrease of capacitance with the increase of current densities was principally owing to an incremental voltage drop and insufficient active material involved in the oxidation/reduction reaction at larger current densities. However, CONTA and COSNP still show a large C_{sp} of 1800 (∼72% retention) and 2360 F/g (∼81% retention) at 20 A/g (see Figure 4c), respectively. The result can be attributed to a huge specific surface area, fluent ion channels and high density active sites of CONTA and COSNP because of the 3D hierarchical nanoarchitecture, which can successfully enhance the utilization and performance of electrodes at large current densities. In contrast, the relatively poor rate capability of the $Co(OH)_2$ electrode is attributed to a diffusion limitation of the ion at large current densities stemming from the time constraints.[34]

As shown in Figure 4d, the long-term stability of CONTA, COSNP, and $Co(OH)_2$ electrodes was measured during charge/discharge cycling through 10 000 cycles at 5 A/g. After 10 000 complete cycles, the $Co(OH)_2$ electrode offered large capacitance loss (about 32%) vs initial capacitance, while CONTA and COSNP electrodes remained stable at 95% and 92% retention, indicating satisfactory cyclic stability of these 3D hierarchical nanoarchitectured electrodes. Figure 4e and f illustrate the electrode after being scanned for 10 000 complete cycles; the results indicate that the developed hierarchical nanoarchitectured structure is preserved upon further cycling. These values are extremely similar to that reported from $Co(OH)_2$ electrodes.[14−22] The nanoporous Ni could perform as the template for restraining the recohesion of $Co(OH)_2$ and support confinement of the active materials, avoiding dissolution or detachment during cycles.[35] The possibility was considered that the Ni is possibly electrochemcally oxidized and contributed to the redox peaks. The improved capacitance was possibly caused by the incorporation of Ni oxide (or hydroxide) into $Co(OH)_2$ through long-term cycles. The great oxidation/reduction current is perhaps also due to the synergistic effect of Co/Ni oxide materials,[36] but further research is required. On the basis of the electrochemical impedance spectroscopy (EIS) curves in Figure S6, this result confirms that the 3D hierarchical nanoarchitectured structure has great electronic/ionic conductivity, which promotes an extremely improved performance.

Good performance is attributed mainly to the unique 3D hierarchical structures of CONTA and COSNP electrodes. Herein, the $Co(OH)_2$ nanorods grown directly on NTA or SNP have some benefits for applications in supercapacitors. (1)

DOI: 10.1021/acsami.5b01163
ACS Appl. Mater. Interfaces 2015, 7, 9147−9156

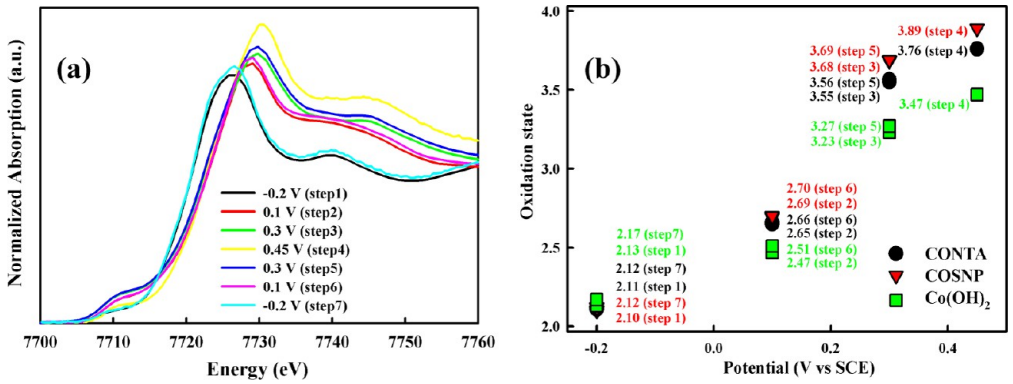

Figure 5. (a) Co K-edge XANES spectra of the COSNP electrode *in situ* measured in KOH solution under various applied potentials. (b) Variation of the Co oxidation state in KOH solution with applied potential.

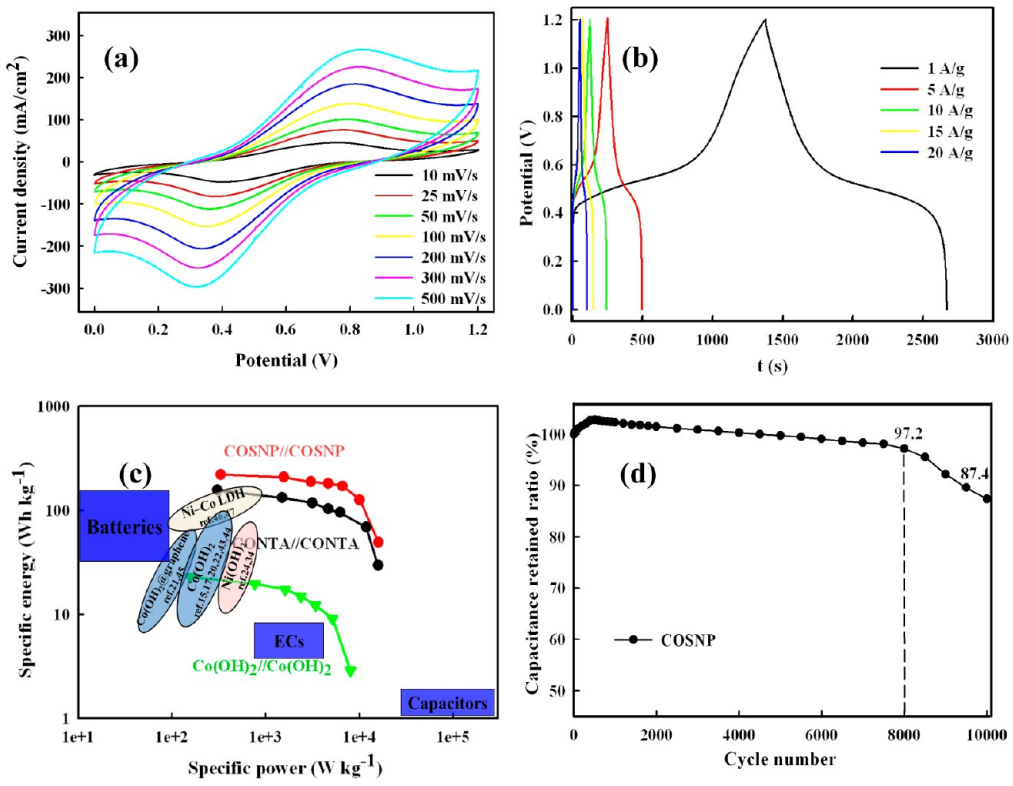

Figure 6. (a) CV curves of the COSNP symmetric supercapacitor at various scan rates in the KOH solution. (b) Galvanostatic charge−discharge curves of the COSNP symmetric supercapacitor at various current densities. (c) Ragone plots of various CONTA, COSNP, and $Co(OH)_2$ symmetric supercapacitors and other hydroxide-based supercapacitors reported in the literature. (d) Long-term cycling performance of symmetric supercapacitor made from the COSNP electrode.

The NTA or SNP substrate with nano/microscale voids/zigzag flow ditches provides the electrode with ultraefficient mass transport and high effective surface area. (2) Every $Co(OH)_2$ nanorod is connected directly to the NTA or SNP framework with successful mechanical adhesion, which produces the quick electron transport pathway and minimizes the interface resistance and further eliminates the demand for conductive additives or binders required in common electrodes. (3) Extremely dispersed $Co(OH)_2$ nanorods further increase the contact area between electrolyte/electrode and assist fast ion diffusion, hence increasing electrochemical kinetics. This micro-, meso-, and macroporous architecture between nanorods provides the OH^- *ion buffering pool*,[23] which confirms that enough of a redox reaction can happen even at a high current density. It also indicates that great C_{sp} is doable at high current densities with the suitably fabricated hierarchical nanoarchitectured framework. High C_{sp} can reduce the oxide amount (the primary cost) applied for the supercapacitor, keeping natural resources. CONTA and COSNP as electrodes thus exhibit superior capacitive performances. The COSNP electrode shows a performance better than that of the CONTA, in terms of C_{sp} and rate capability, but CONTA has a lower surface area (~30%) than COSNP. Except surface area, a perfect nanostructure of the electrode is of key importance to achieve efficient electron transport. In Figure 1, SNP substrates provide many pathways for ion diffusion and electron transport, therefore increasing their pseudocapacitive performance. To

DOI: 10.1021/acsami.5b01163
ACS Appl. Mater. Interfaces 2015, 7, 9147−9156

confirm the notion, we studied pseudocapacitive characteristics of all electrodes in solution with *in situ* XANES.

Figure 5a displays Co K-edge XANES spectra of COSNP *in situ* studied under seven potentials in the sequence −0.2 V, +0.1 V, +0.3 V, +0.45 ,V then +0.3 V, +0.1 V, and finally −0.2 V. The XANES spectra of the COSNP electrode shifted to larger energy with enhancing the potential and backtracked practically to the early place as the potential was inverted. According to threshold energy (E_0) derived from XANES spectra in Figure 5a,[37,38] the average oxidation state of the COSNP electrode in solution was established in a sequence displayed in Figure 5b. (Co, CoO(II), Co_3O_4, Co_2O_3(III), and CoO_2(IV) were also analyzed, respectively.) Figure 5b shows the average oxidation state of Co ions deduced from Co K-edge XANES spectra of the COSNP, CONTA, and $Co(OH)_2$ electrodes in the sequence −0.2 V, +0.1 V, +0.3 V, +0.45 V, then +0.3 V, +0.1 V, and finally −0.2 V in KOH solution, respectively. The change of Co oxidation state from −0.2 V to +0.45 V with COSNP is about 1.79, which is higher than that with CONTA and $Co(OH)_2$. These results confirm that the 3D nanoporous structure reduces the distances of ionic/electronic transport in COSNP and then enhances the kinetic capability, promoting the significant C_{sp} seen in Figure 4, which is the key factor for an ideal electrochemical capacitor.

3.3. Building Symmetric Supercapacitors. To evaluate their practical applications, we assembled a symmetric supercapacitor using our electrodes as cathode and anode electrodes,[39−42] as illustrated in Figure S7. In preparation of symmetric supercapacitors, all weights of positive/negative electrodes were optimized according to the single electrode measurement results to guarantee more efficient utilization of the active materials. Figure 6a shows the CV of the COSNP symmetric supercapacitor at different scan rates. The redox peaks on the CV are watched; the current increases with the scan rate increasing from 10 to 500 mV/s, but there is no significant distortion of CV even at 500 mV/s, meaning the rapid charge/discharge characteristics of this device. These CV curves shown in Figure 6a also show that cell voltage of this device can be as high as 1.2 V. To further assess the cell performance, we performed charging and discharging tests at different current densities; the results are shown in Figure 6b. The device was able to deliver a high C_{sp} of 1100 F/g (based on total mass of electroactive materials) at 1 A/g and 850 F/g at 20 A/g. According to the results, we determined energy density (E) and power density (P) of symmetric supercapacitor devices; these relationships between energy and power are displayed as a Ragone plot in Figure 6c. With galvanostatic charge/discharge plots based on two-electrode cells, the C_{sp} of a single electrode, the E, and the P were established from chronopotentiometric curves according to[12,39,40]

$$E = 1/2C_{sp}\Delta V^2 \quad (5)$$

$$P = E/\Delta t \quad (6)$$

where ΔV is cell voltage (i.e., 1.2 V) and Δt is time to full charge (or discharge). The COSNP symmetric supercapacitor exhibited an ultrahigh energy density of 220 Wh/kg at a low power density of 0.3 kW/kg and a high power density of 16 kW/kg at an energy density of 49 Wh/kg. Maximum energy densities of CONTA and $Co(OH)_2$ symmetric supercapacitor are 156 Wh/kg (0.3 kW/kg) and 23 Wh/kg (0.2 kW/kg), respectively. Especially remarkable is that maximum energy density acquired from the COSNP symmetric supercapacitor is significantly greater than those of supercapacitors based on amorphous $Co(OH)_2$ (54.7 Wh/kg),[18] $Co(OH)_2$ nanostructures (19.5−85 Wh/kg),[15,17,19,20,22,43,44] $Co(OH)_2$@graphene (16.5−40.8 Wh/kg),[21,45] $Co(OH)_2$@ionic liquid (37.6 Wh/kg),[16] amorphous $Ni(OH)_2$//AC (12.6 Wh/kg),[34] $Ni(OH)_2$/Ni foam (82.7 Wh/kg),[24] Ni_xCo_{1-x} LDH@ZTO//AC (23.7 Wh/kg),[46] Ni−Co LDH//RGO (188 Wh/kg),[47] and oxyhydroxide@nanoporous Ni−Mn (28.1 Wh/kg).[48] The COSNP symmetric supercapacitor shows great long-cycle stability even at 5 A/g as shown in Figure 6d (∼87% of initial C_{sp} after 10 000 cycles). These findings indicate that COSNP and CONTA are hopeful electrodes for supercapacitors with superior performance and might open huge opportunities for electrochemical energy conversion and storage devices.

4. CONCLUSION

$Co(OH)_2$-based supercapacitor electrodes of low cost and large area were fabricated through an easy and template-assisted deposition followed by a facile electrochemical method. The procedure involves the electrodeposition of Cu/Ni film on nickel foam, etching of Cu from the Cu/Ni layer (leaving Ni nanotube arrays or sucker-like Ni nanoporous films, respectively), and cathodic deposition of $Co(OH)_2$ on nanoporous Ni substrates. Because of their unique 3D nanostructures, the CONTA and COSNP electrodes exhibited specific capacitances of 2500 and 2900 F/g at 1 A/g, respectively, and outstanding long-cycle stability, a retention of 95% and 92% after 10 000 cycles. The symmetric supercapacitor based on the COSNP as electrodes were assembled; it exhibited a C_{sp} of 1100 F/g at 1 A/g and a high E of 220 Wh/kg. Moreover, the device has outstanding cycle stability—only 13% loss after 10 000 cycles, making it promising as an attractive candidate for electrochemical energy storage devices.

■ ASSOCIATED CONTENT

Ⓢ Supporting Information

CV curves of the nickel foam electrode in a plating solution; XPS of Ni−Cu electrodes; SEM image of $Co(OH)_2$ nanoflakes electrode; nitrogen adsorption/desorption isotherms of CONTA and $Co(OH)_2$ electrodes; galvanostatic charge/discharge cycles of COSNP at different current densities; Nyquist plots of CONTA, COSNP, and $Co(OH)_2$ electrodes. This material is available free of charge via the Internet at http://pubs.acs.org.

■ AUTHOR INFORMATION

Corresponding Authors

*E-mail: deng.mj@nsrrc.org.tw or martinez730523@yahoo.com.tw.

*E-mail: jmchen@nsrrc.org.tw.

*E-mail: ktlu@nsrrc.org.tw.

Author Contributions

§These authors contributed equally to this work.

Notes

The authors declare no competing financial interest.

■ ACKNOWLEDGMENTS

The authors sincerely acknowledge the financial support from NSRRC and Ministry of Science and Technology (Taiwan; grant numbers: MOST102-2113-M-213-004-MY3 and MOST103-2113-M-213-004).

DOI: 10.1021/acsami.5b01163
ACS Appl. Mater. Interfaces 2015, 7, 9147−9156

REFERENCES

(1) Miller, J. R.; Simon, P. Electrochemical Capacitors for Energy Management. *Science* **2008**, *321*, 651−652.

(2) Simon, P.; Gogotsi, Y. Materials for Electrochemical Capacitors. *Nat. Mater.* **2008**, *7*, 845−854.

(3) Wang, Z. L.; Wu, W. Nanotechnology-Enabled Energy Harvesting for Self-Powered Micro-/Nanosystems. *Angew. Chem., Int. Ed.* **2012**, *51*, 11700−11721.

(4) Wang, G. P.; Zhang, L.; Zhang, J. J. A Review of Electrode Materials for Electrochemical Supercapacitors. *Chem. Soc. Rev.* **2012**, *41*, 797−828.

(5) Beidaghi, M.; Gogotsi, Y. Capacitive Energy Storage in Micro-scale Devices: Recent Advances in Design and Fabrication of Micro-supercapacitors. *Energy Environ. Sci.* **2014**, *7*, 867−884.

(6) Zhao, L.; Hu, Y. S.; Li, H.; Wang, Z.; Chen, L. Porous $Li_4Ti_5O_{12}$ Coated with N-Doped Carbon from Ionic Liquids for Li-Ion Batteries. *Adv. Mater.* **2011**, *23*, 1385−1388.

(7) An, K. H.; Kim, W. S.; Park, Y. S.; Moon, J. M.; Bae, D. J.; Lim, S. C.; Lee, Y. S.; Lee, Y. H. Electrochemical Properties of High-Power Supercapacitors Using Single-Walled Carbon Nanotube Electrodes. *Adv. Funct. Mater.* **2001**, *11*, 387−392.

(8) Xu, Z. W.; Li, Z.; Holt, C. M. B.; Tan, X. H.; Wang, H. L.; Amirkhiz, B. S.; Stephenson, T.; Mitlin, D. Electrochemical Super-capacitor Electrodes from Sponge-like Graphene Nanoarchitectures with Ultrahigh Power Density. *J. Phys. Chem. Lett.* **2012**, *3*, 2928−2933.

(9) Wang, K.; Wang, Y.; Wang, Y.; Hosono, E.; Zhou, H. Mesoporous Carbon Nanofibers for Supercapacitor Application. *J. Phys. Chem. C* **2009**, *113*, 1093−1097.

(10) Chang, K. H.; Hu, C. C.; Chou, C. Y. Textural and Capacitive Characteristics of Hydrothermally Derived $RuO_2{\cdot}xH_2O$ Nanocrystal-lites: Independent Control of Crystal Size and Water Content. *Chem. Mater.* **2007**, *19*, 2112−2119.

(11) Hu, C. C.; Chang, K. H.; Lin, M. C.; Wu, Y. T. Design and Tailoring of the Nanotubular Arrayed Architecture of Hydrous RuO_2 for Next Generation Supercapacitors. *Nano Lett.* **2006**, *6*, 2690−2695.

(12) Rakhi, R. B.; Chen, W.; Cha, D.; Alshareef, H. N. Substrate Dependent Self-Organization of Mesoporous Cobalt Oxide Nanowires with Remarkable Pseudocapacitance. *Nano Lett.* **2012**, *12*, 2559−2567.

(13) Chang, J. K.; Wu, C. M.; Sun, I. W. Nano-architectured $Co(OH)_2$ Electrodes Constructed Using an Easily-Manipulated Electrochemical Protocol for High-Performance Energy Storage Applications. *J. Mater. Chem.* **2010**, *20*, 3729−3735.

(14) Cao, L.; Xu, F.; Liang, Y. Y.; Li, H. L. Preparation of the Novel Nanocomposite $Co(OH)_2$/Ultra-Stable Y Zeolite and Its Application as a Supercapacitor with High Energy Density. *Adv. Mater.* **2004**, *16*, 1853−1857.

(15) Xue, T.; Lee, J. M. Capacitive Behavior of Mesoporous $Co(OH)_2$ Nanowires. *J. Power Sources* **2014**, *245*, 194−202.

(16) Choi, B. G.; Yang, M.; Jung, S. C.; Lee, K. G.; Kim, J. G.; Park, H.; Park, T. J.; Lee, S. B.; Han, Y. K.; Huh, Y. S. Enhanced Pseudocapacitance of Ionic Liquid/Cobalt Hydroxide Nanohybrids. *ACS Nano* **2013**, *7*, 2453−2460.

(17) Mondal, C.; Ganguly, M.; Manna, P. K.; Yusuf, S. M.; Pal, T. Fabrication of Porous β-$Co(OH)_2$ Architecture at Room Temper-ature: A High Performance Supercapacitor. *Langmuir* **2013**, *29*, 9179−9187.

(18) Li, H. B.; Yu, M. H.; Lu, X. H.; Liu, P.; Liang, Y.; Xiao, J.; Tong, Y. X.; Yang, G. W. Amorphous Cobalt Hydroxide with Superior Pseudocapacitive Performance. *ACS Appl. Mater. Interfaces* **2014**, *6*, 745−749.

(19) Li, M.; Xu, S.; Liu, T.; Wang, F.; Yang, P.; Wang, L.; Chub, P. K. Electrochemically-deposited Nanostructured $Co(OH)_2$ Flakes on Three-Dimensional Ordered Nickel/Silicon Microchannel Plates for Miniature Supercapacitors. *J. Mater. Chem. A* **2013**, *1*, 532−540.

(20) Gupta, V.; Kusahara, T.; Toyama, H.; Gupta, S.; Miura, N. Potentiostatically Deposited Nanostructured α-$Co(OH)_2$: A High Performance Electrode Material for Redox-Capacitors. *Electrochem. Commun.* **2007**, *9*, 2315−2319.

(21) Li, Z.; Wang, J.; Niu, L.; Sun, J.; Gong, P.; Hong, W.; Ma, L.; Yang, S. Rapid Synthesis of Graphene/Cobalt Hydroxide Composite with Enhanced Electrochemical Performance for Supercapacitors. *J. Power Sources* **2014**, *245*, 224−231.

(22) Pan, G. X.; Xia, X.; Cao, F.; Tang, P. S.; Chen, H. F. Porous $Co(OH)_2$/Ni Composite Nanoflake Array for High Performance Supercapacitors. *Electrochim. Acta* **2012**, *63*, 335−340.

(23) Yuan, C.; Yang, L.; Hou, L.; Shen, L.; Zhang, X.; Lou, X. W. Growth of Ultrathin Mesoporous Co_3O_4 Nanosheet Arrays on Ni Foam for High-performance Electrochemical Capacitors. *Energy Environ. Sci.* **2012**, *5*, 7883−7887.

(24) Xiong, X.; Ding, D.; Chen, D.; Waller, G.; Bu, Y.; Wang, Z.; Liu, M. Three-dimensional Ultrathin $Ni(OH)_2$ Nanosheets Grown on Nickel Foam for High Performance Supercapacitors. *Nano Energy* **2015**, *11*, 154−161.

(25) Jiang, J.; Li, Y.; Liu, J.; Huang, X.; Yuan, C.; Lou, X. W. Recent Advances in Metal Oxide-based Electrode Architecture Design for Electrochemical Energy Storage. *Adv. Mater.* **2012**, *24*, 5166−5180.

(26) Liu, J.; Zhang, L.; Wu, H. B.; Lin, J.; Shen, Z.; Lou, X. W. High-Performance Flexible Asymmetric Supercapacitors Based on A New Graphene Foam/Carbon Nanotube Hybrid Film. *Energy Environ. Sci.* **2014**, *7*, 3709−3719.

(27) Gao, G.; Wu, H. B.; Ding, S.; Liu, L. M.; Lou, X. W. Hierarchical $NiCo_2O_4$ Nanosheets Grown on Ni Nanofoam as High-Performance Electrodes for Supercapacitors. *Small* **2015**, *11*, 804−808.

(28) Wang, H. Y.; Xiao, F. X.; Yu, L.; Liu, B.; Lou, X. W. Hierarchical α-MnO_2 Nanowires@$Ni_{1-x}Mn_xO_y$ Nanoflakes Core-Shell Nanostruc-tures for Supercapacitors. *Small* **2014**, *10*, 3181−3186.

(29) Nelson, P. A.; Elliott, J. M.; Attard, G. S.; Owen, J. R. Mesoporous Nickel/Nickel Oxide- a Nanoarchitectured Electrode. *Chem. Mater.* **2002**, *14*, 524−529.

(30) Marcus, P.; Bussell, M. E. XPS Study of the Passive Films Formed on Nitrogen-Implanted Austenitic Stainless Steels. *Appl. Surf. Sci.* **1992**, *59*, 7−21.

(31) Sun, L.; Chien, C. L.; Searson, P. C. Fabrication of Nanoporous Nickel by Electrochemical Dealloying. *Chem. Mater.* **2004**, *16*, 3125−3129.

(32) Liu, Z.; Elbert, D.; Chien, C. L.; Searson, P. C. FIB/TEM Characterization of the Composition and Structure of Core/Shell Cu−Ni Nanowires. *Nano Lett.* **2008**, *8*, 2166−2170.

(33) Yang, J.; Liu, H. W.; Martens, W. N.; Frost, R. L. Synthesis and Characterization of Cobalt Hydroxide, Cobalt Oxyhydroxide, and Cobalt Oxide Nanodiscs. *J. Phys. Chem. C* **2010**, *114*, 111−119.

(34) Li, H. B.; Yu, M. H.; Wang, F. X.; Liu, P.; Liang, Y.; Xiao, J.; Wang, C. X.; Tong, Y. X.; Yang, G. W. Amorphous Nickel Hydroxide Nanospheres with Ultrahigh Capacitance and Energy Density as Electrochemical Pseudocapacitor Materials. *Nat. Commun.* **2013**, *4*, 1894−1900.

(35) Deng, M. J.; Huang, F. L.; Sun, I. W.; Tsai, W. T.; Chang, J. K. An Entirely Electrochemical Preparation of a Nano-Structured Cobalt Oxide Electrode with Superior Redox Activity. *Nanotechnology* **2009**, *20*, 175602.

(36) He, K. X.; Wu, Q. F.; Zhang, X. G.; Wang, X. L. Electrodeposition of Nickel and Cobalt Mixed Oxide/Carbon Nanotube Thin Films and Their Charge Storage Properties. *J. Electrochem. Soc.* **2006**, *153*, A1568−A1574.

(37) Okumura, T.; Yamaguchi, Y.; Shikano, M.; Kobayashi, H. Correlation of Lithium Ion Distribution and X-ray Absorption Near-edge Structure in O_3- and O_2-Lithium Cobalt Oxides from First-principle Calculation. *J. Mater. Chem.* **2012**, *22*, 17340−17348.

(38) Hwang, B. J.; Tsai, Y. W.; Sarma, L. S.; Chen, C. H.; Lee, J. F.; Strehblow, H. H. In Situ XAS Investigation of Transformation of Co Monolayer on Carbon-Supported Platinum Clusters Underpotential Control. *J. Phys. Chem. B* **2004**, *108*, 15096−15102.

(39) Dong, C.; Wang, Y.; Xu, J.; Cheng, G.; Yang, W.; Kou, T.; Zhang, Z.; Ding, Y. 3D Binder-Free Cu_2O@Cu Nanoneedle Arrays for High-performance Asymmetric Supercapacitors. *J. Mater. Chem. A* **2014**, *2*, 18229−18235.

DOI: 10.1021/acsami.5b01163
ACS Appl. Mater. Interfaces 2015, 7, 9147−9156

(40) Liu, C.; Yu, Z.; Neff, D.; Zhamu, A.; Jang, B. Z. Graphene-Based Supercapacitor with an Ultrahigh Energy Density. *Nano Lett.* **2010**, *10*, 4863−4868.
(41) Gao, X. P.; Yao, S. M.; Yan, T. Y.; Zhou, Z. Alkaline Rechargeable Ni/Co Batteries: Cobalt Hydroxides as Negative Electrode Materials. *Energy Environ. Sci.* **2009**, *2*, 502−505.
(42) Wu, X.; Lu, Z.; Zhu, W.; Yang, Q.; Zhang, G.; Liu, J.; Sun, X. High-Performance Aqueous Battery with Double Hierarchical Nanoarrays. *Nano Energy* **2014**, *10*, 229−234.
(43) Cao, F.; Pan, G. X.; Tang, P. S.; Chen, H. F. Hydrothermal-Synthesized $Co(OH)_2$ Nanocone Arrays for Supercapacitor Application. *J. Power Sources* **2012**, *216*, 395−399.
(44) Jiang, J.; Liu, J. P.; Ding, R. M.; Zhu, J. H.; Li, Y. Y.; Hu, A. Z.; Li, X.; Huang, X. T. Large-Scale Uniform α-$Co(OH)_2$ Long Nanowire Arrays Grown on Graphite as Pseudocapacitor Electrodes. *ACS Appl. Mater. Interfaces* **2011**, *3*, 99−103.
(45) Chen, S.; Zhu, J. W.; Wang, X. One-Step Synthesis of Graphene−Cobalt Hydroxide Nanocomposites and Their Electrochemical Properties. *J. Phys. Chem. C* **2010**, *114*, 11829−11834.
(46) Wang, X.; Sumboja, A.; Lin, M.; Yan, J.; Lee, P. S. Enhancing Electrochemical Reaction Sites in Nickel−Cobalt Layered Double Hydroxides on Zinc Tin Oxide Nanowires: A Hybrid Material for An Ssymmetric Supercapacitor Device. *Nanoscale* **2012**, *4*, 7266−7272.
(47) Chen, H.; Hu, L.; Chen, M.; Yan, Y.; Wu, L. Nickel−Cobalt Layered Double Hydroxide Nanosheets for High-performance Supercapacitor Electrode Materials. *Adv. Funct. Mater.* **2014**, *24*, 934−942.
(48) Kang, J. L.; Hirata, A.; Qiu, H. J.; Chen, L. Y.; Ge, X. B.; Fujita, T.; Chen, M. W. Self-Grown Oxy-Hydroxide@Nanoporous Metal Electrode for High-Performance Supercapacitors. *Adv. Mater.* **2013**, *26*, 269−272.

DOI: 10.1021/acsami.5b01163
ACS Appl. Mater. Interfaces 2015, 7, 9147−9156